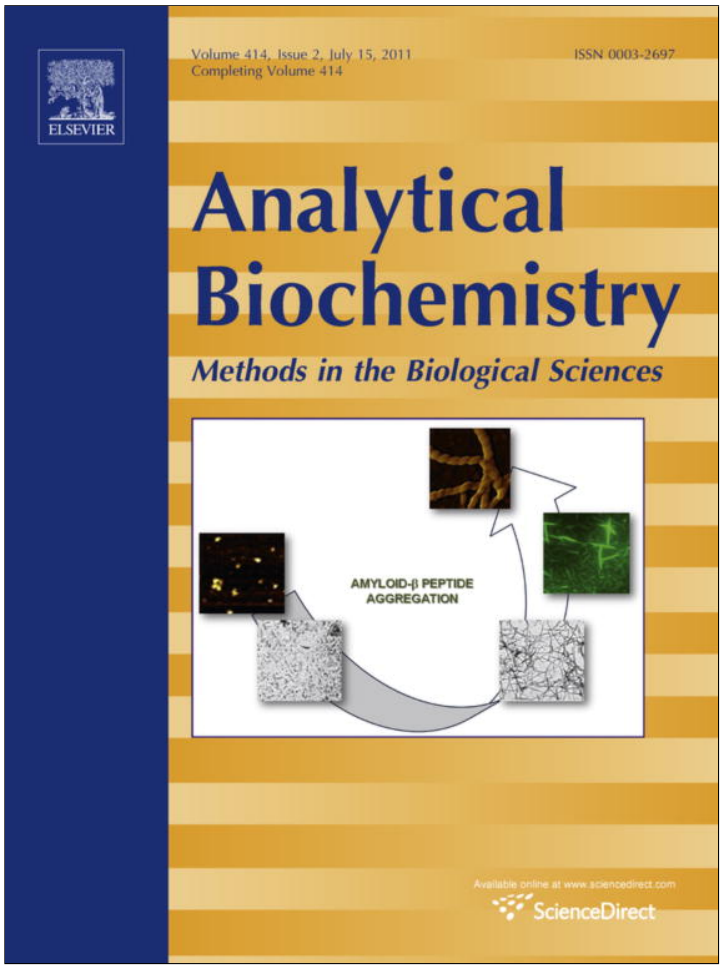

Analytical Biochemistry 414 (2011) 215–225

Contents lists available at ScienceDirect

Analytical Biochemistry

journal homepage: www.elsevier.com/locate/yabio

Kinetic characterization of amyloid-beta 1–42 aggregation with a multimethodological approach

Manuela Bartolini [a,1], Marina Naldi [a,1], Jessica Fiori [a], Francesco Valle [b], Fabio Biscarini [b], Dan V. Nicolau [c], Vincenza Andrisano [a,*]

[a] Department of Pharmaceutical Sciences, University of Bologna, 40126 Bologna, Italy
[b] Institute for Nanostructured Materials, CNR, 40129 Bologna, Italy
[c] Department of Electrical Engineering and Electronics, University of Liverpool, Liverpool, L69 3GJ, UK

ARTICLE INFO

Article history:
Received 12 January 2011
Received in revised form 16 March 2011
Accepted 17 March 2011
Available online 22 March 2011

Keywords:
Amyloid-beta peptide
Self-aggregation
Atomic force microscopy
MALDI–TOF mass spectrometry
Myricetin

ABSTRACT

Extensive evidence suggests that the self-assembly of amyloid-beta peptide (Aβ) is a nucleation-dependent process that involves the formation of several oligomeric intermediates. Despite neuronal toxicity being recently related to Aβ soluble oligomers, results from aggregation studies are often controversial, mainly because of the low reproducibility of several experimental protocols. Here a multimethodological study that included atomic force microscopy (AFM), transmission electron microscopy (TEM), fluorescence microscopy (FLM), mass spectrometry techniques (matrix-assisted laser desorption/ionization time-of-flight [MALDI–TOF] and electrospray ionization quadrupole time-of-flight [ESI–QTOF]), and direct thioflavin T (ThT) fluorescence spectroscopy were enabled to set up a reliable and highly reproducible experimental protocol for the characterization of the morphology and dimension of Aβ 1–42 (Aβ42) aggregates along the self-assembly pathway. This multimethodological approach allowed elucidating the diverse assembly species formed during the Aβ aggregation process and was applied to the detailed investigation of the mechanism of Aβ42 inhibition by myricetin. In particular, a very striking result was the molecular weight determination of the initial oligomeric nuclei by MALDI–TOF, composed of up to 10 monomers, and their morphology by AFM.

Aggregation and fibril formation of amyloid-beta peptide (Aβ)[2] are central events in the pathogenesis and progression of Alzheimer's disease (AD) [1,2]. Aβ occurs in various isoforms that differ by the number of amino acids at the C terminus [3]. Specifically, the 40-residue (Aβ40) and 42-residue (Aβ42) isoforms both have been associated with AD. In particular, Aβ42 shows a high propensity to self-assemble and deposit in senile plaques and is highly toxic for neurons [4], and its overproduction has been related to familiar forms of AD [5]. Aggregation of Aβ42 is a complex process that involves the formation of several soluble intermediate species, including oligomeric and protofibrillar forms, and ends with the deposition of ordered fibrillar architectures whose three-dimensional structure has been recently published [6]. The process of in vivo polymerization is poorly understood, and the pathological role of different soluble species is still controversial. For instance, although the amyloid plaques are a major hallmark of AD, they are only part of an array of Aβ aggregate morphologies observed in vivo [7]. Interestingly, not all of these Aβ assemblies provoke an inflammatory response and are toxic. The detailed pathological mechanism still remains unclear. Considerable evidence suggests that soluble ordered oligomeric intermediates (e.g., soluble oligomers [56 kDa] and protofibrils), rather than insoluble peptide deposits, exert cytotoxic effects and play a crucial role in AD onset and progression [8–10]. Aβ deposits may enhance oxidative stress and inflammation, leading to cell injury [11].

Despite this acute importance and interest, there are several aspects of amyloid aggregation that conspire against reliable experimental studies and direct comparison of the results. First, the kinetics of Aβ42 aggregation is very sensitive to inputs, such as the conformational status of starting material [12] and physicochemical characteristics of the solution [13], and studies are limited by the poor water solubility of Aβ42. Indeed, depending on experimental conditions and the detection system, different on- and off-pathway intermediates have been reported, resulting

* Corresponding author. Fax: +39 051 2099734.
E-mail address: vincenza.andrisano@unibo.it (V. Andrisano).

[1] These authors contributed equally to this research.

[2] *Abbreviations used:* Aβ, amyloid-beta peptide; AD, Alzheimer's disease; CD, circular dichroism; MS, mass spectrometry; MALDI–TOF, matrix-assisted laser desorption/ionization time-of-flight; ESI–IT, electrospray ionization ion trap; ESI–QTOF, electrospray ionization quadrupole time-of-flight; ThT, thioflavin T; TEM, transmission electron microscopy; FLM, fluorescence microscopy; AFM, atomic force microscopy; IS, internal standard; LC–MS, liquid chromatography mass spectrometry; SIM, single ion monitoring; HFIP, hexafluoroisopropanol; CD, circular dichroism; HMW, high-molecular-weight; PICUP, photo-induced cross-linking of unmodified proteins; MW, molecular weight; LMW, low-molecular-weight.

0003-2697/$ - see front matter © 2011 Elsevier Inc. All rights reserved.
doi:10.1016/j.ab.2011.03.020

in divergent kinetics and aggregation models [13–15]. Second, the structural polymorphism (i.e., the tendency to aggregate into multiple morphologies, which is a prominent feature of Aβ aggregation) makes the reliable in vitro reproduction of neurotoxicity-related assembly difficult, thereby leading to contradictory study outcomes.

Beside dissimilarity related to nonreproducible aggregation kinetics, this heterogeneity translated to confused outcomes from screening procedures for inhibitors, hampering the rational design of new drugs for AD. The case of nicotine is emblematic; each D-(+) and L-(−) enantiomer of nicotine was reported to inhibit Aβ aggregation and related cytotoxicity [16] despite the fact that the racemate was previously found to be inactive [17].

Given the importance of these aspects as well as the intrinsic and experimental difficulties related to this process, our objective was to develop a more comprehensive methodology to characterize the formation of amyloid aggregates. This objective has been achieved by combining the development of a reproducible aggregation assay with a multimethodological detection approach for the evaluation of alternative Aβ42 morphology and aggregation species associated with various steps of the aggregation pathway. Apart from helping to clarify the aggregation mechanism, this information is also crucial to understanding where potential Aβ aggregation inhibitors act along the aggregation pathway, thereby aiding in the design of new effective drugs for the treatment of AD.

Numerous analytical techniques have been used to evaluate the Aβ aggregation process in vitro. These include direct nonmorphological methods such as circular dichroism (CD) [18] and solid-state and liquid nuclear magnetic resonance (NMR) [19], indirect morphological techniques such as colorimetric [20] and fluorometric methods [21], and morphological methods such as turbidity, light scattering, and X-ray diffraction microscopy [22]. Application of each of these techniques offers advantages and may have drawbacks in terms of technique-related artifacts, which might be related to sample treatment (e.g., required filtration), staining (e.g., negative stain in electron microscopy), surface- or assay-induced assembly or disassembly (e.g., sodium dodecyl sulfate–polyacrylamide gel electrophoresis [SDS–PAGE] fractionation) [23], or a lack of selectivity of detection system for oligomer determination (e.g., cross reaction in some immunoassays) [24].

In our opinion, these artifacts can be overcome by using multiple independent analytical techniques in parallel. Therefore, in this work, we extended our previous studies [18] by combining mass spectrometry (MS) techniques (matrix-assisted laser desorption/ionization time-of-flight [MALDI–TOF], electrospray ionization ion trap [ESI–IT], and electrospray ionization quadrupole time-of-flight [ESI–QTOF]), thioflavin T (ThT)-based fluorescence spectroscopy, and microscopy techniques such as transmission electron microscopy (TEM), fluorescence microscopy (FLM), and atomic force microscopy (AFM). These methodologies were applied to monitor in parallel the oligomerization of conformationally homogeneous samples and were used to cross-validate results. Comparison of results minimized the misinterpretation related to technique-induced phenomena (e.g., surface-induced aggregation), leading to artifact-free outcomes. Different combinations of analytical methods have been approached previously [25–29]. However, transient species appearing at an early phase of the Aβ42 oligomerization process have been hardly characterized. The MALDI–TOF technique was successfully selected for this purpose in this study. Furthermore, ESI–IT MS and ESI–QTOF MS were applied for the first time for measuring the progressive disappearance of monomer during inhibition studies with the known Aβ inhibitor myricetin. The final goal of this work was to understand the in vitro Aβ42 self-assembly process so as to intervene along the aggregation path by a concurrent inhibitor. This work gives further opportunities for a reliable assay on amyloid aggregation and contributes to the understanding of the detailed mechanism of the action of inhibitors.

Materials and methods

Aβ42 sample preparation

Aβ42 lyophilized powder (Bachem, Bubendorf, Switzerland) was pretreated and resolubilized following the procedure optimized in a previous work and slightly adapted for the current studies [14]. The Aβ42 film was redissolved in 69.5 μl of a freshly prepared mixture consisting of CH_3CN/300 μM Na_2CO_3/250 mM NaOH (48.3:48.3:3.4, v/v/v) by brief sonication and vortexing. The resulting alkaline Aβ42 solution (500 μM) was diluted 1:10 with phosphate buffer (10 mM, pH 7.7) containing NaCl (11 mM) to obtain a 50-μM Aβ42 solution at final pH 8.0 and an NaCl concentration of 10 mM. Therefore, final assay conditions were as follows: 50 μM Aβ42 in phosphate buffer (8.7 mM) containing 10 mM NaCl, 14.5 μM Na_2CO_3, 0.85 mM NaOH, and 8.2% acetonitrile (final pH 8.0). The Aβ42 solutions were briefly sonicated and incubated at 30 °C by a Thermomixer Comfort (Eppendorf Italia, Milan, Italy) without any stirring. Analyses were then performed at selected times.

Aβ42 aggregation inhibition studies

Inhibition studies were performed by incubating Aβ42 samples at 30 °C without any stirring in the assay conditions with and without myricetin. Myricetin was solubilized in methanol at a stock concentration of 2.0 mM and diluted in the assay buffer. For the evaluation of IC_{50} value, four different concentrations (1.0–10 μM) were used. IC_{50} value was determined graphically from log concentration–inhibition curves (GraphPad Prism 4.03, GraphPad Software, San Diego, CA, USA). In time course experiments, stock solution was diluted in the assay buffer to a final concentration of 10 μM ([myricetin]/[Aβ42] = 1:5). At $t = 0$, aliquots of stock solution were added to the Aβ42 samples before incubation at 30 °C. In further studies, myricetin was added during the aggregation process at selected times (t_{50} [half-time course in ThT assay] and t_{90} [90% of the exponential increase of the fluorescence signal in the ThT assay]). At selected times, aliquots were analyzed for Aβ42 on the specific technique-related protocol in the specific sections reported below. Inhibition studies with tacrine were carried out by preparing a 2.0-mM stock solution of tacrine hydrochloride (Sigma–Aldrich, Milan, Italy) in methanol and diluting it in the assay buffer to have a final concentration of 10 μM. At $t = 0$, aliquots of tacrine solution were added to the Aβ42 samples before incubation at 30 °C.

ThT-based fluorometric assay

ThT (Sigma–Aldrich)-based fluorometric assays were performed with a Jasco FP-6200 spectrofluorometer (Jasco, Tokyo, Japan) using a 3-ml quartz cell. After the appropriate incubation time, the solutions containing Aβ42 (50 μM) or Aβ42 in the presence of myricetin were diluted with glycine–NaOH buffer (50 mM, pH 8.5) containing ThT (1.5 μM) up to a final volume of 2.0 ml. The fluorescence emission signal was monitored at 490 nm (λ_{ex} = 446 nm) with excitation and emission slits of 2 nm bandwidth. A time scan was performed, and the fluorescence intensity values at the plateau (∼300 s) were averaged after subtracting the background fluorescence from 1.5 μM ThT and tested compound.

MALDI–TOF

Aβ42 MALDI–TOF MS analyses were performed using a Voyager DE Pro (Applied Biosystems, Foster City, CA, USA) equipped with a pulsed nitrogen laser operating at 337 nm. Small oligomer positive ion spectra were acquired in linear mode over an m/z range from 2000 to 50,000 using a 25-kV accelerating voltage, a 23.25-kV grid voltage, and a 400-ns delay extraction time. The spectrum for each spot was obtained by averaging the results of 1000 laser shots. The analysis was performed by spotting on the target plate 1.0 μl of the sample mixed with an equal volume of the matrix solution, 30 mg/ml sinapinic acid (Sigma-Aldrich), in CH_3CN/H_2O (50:50, v/v) containing 0.1% (v/v) trifluoroacetic acid (Sigma–Aldrich).

ESI–IT MS

The Aβ42 samples were analyzed by a 10-μl loop injection after previous addition of reserpine (Sigma–Aldrich) as internal standard (IS) (2 μl of 0.5 mg/ml IS in 2:1 acetonitrile/phosphate buffer was added to 20 μl of Aβ42 solution). Liquid chromatography mass spectrometry (LC–MS) analyses were performed on a Jasco PU-1585 liquid chromatograph interfaced with an LCQ Duo mass spectrometer (Thermo Finnigan, San Jose, CA, USA) equipped with an ESI source operating with an ion trap analyzer. The mobile phase consisted of 0.1% (v/v) formic acid in acetonitrile/water (30:70). The ESI system employed a 4.5-kV spray voltage and a 200 °C capillary temperature. Mass spectra were operated in positive polarity in a scan range of 200 to 2000 m/z and at a scan rate of 3 microscans/s. Single ion monitoring (SIM) chromatograms for the quantitative analysis were reconstructed at the base peaks corresponding to the differentially charged amyloid monomer ions. In particular, the responses due to the ESI generated different charge states of the monomer (ions $[M+4H]^{4+}$ at 1129.3 m/z, $[M+5H]^{5+}$ at 903.7 m/z, and $[M+6H]^{6+}$ at 753.3 m/z) were summarized as total monomer SIM area. The ratio between the monomer area, calculated as described previously, and the IS area (SIM at 609.4 m/z, corresponding to $[M+H]^+$ reserpine ion) was used for quantitation.

AFM

The AFM samples were prepared by spotting 8 μl of Aβ42 solution on freshly cleaved muscovite mica disks (Joel, Milan, Italy). The contact time was 1 min; mica disks were then rinsed with 0.22-μm filtered deionized water and gently dried under a nitrogen flow. Morphological analysis was carried out with an NT–MDT atomic force microscope (SMENA NOVA, NT–MDT, Moscow, Russia) in semicontact mode, in air, under the following conditions: scan rate 1–1.5 Hz, NSG11 golden silicon probes (NT–MDT) with tip apex radius of 10 nm, resonant frequency range of AFM cantilever 115–325 Hz, and number of pixels 512 × 512. Representative images were obtained by scanning different samples at three or more randomly selected spots over the entire template. The resulting images were processed off-line with Gwiddion 2.17 software (http://gwyddion.net) by applying a flattening algorithm to remove the background slope. For width measurement of small structures, such as amyloid small aggregates, complex algorithms are usually required to deconvolute the images [30]. A good estimation of the real size of the small oligomers can be obtained by a simple geometrical deconvolution model [28,31], that is, by treating the small particles as spherical structures and the small protofibrils and fibrils as cylindrical structures:

$$w = 2 \cdot (2 \cdot R_t \cdot h)1/2 \quad (1)$$

where w is the width or diameter observed in the AFM image, R_t is the tip apex radius (10 nm), and h is the real width of the structure.

TEM

Aliquots (2 μl) of the Aβ42 samples diluted 10 times in the assay buffer were adsorbed onto 200-mesh carbon-coated copper grids (Electron Microscopy Sciences, Hatfield, PA, USA) until dry. The grids were then washed three times with filtered bidistilled water, stained with 1% aqueous solution of uranyl acetate (Sigma–Aldrich) for 5 min, and finally washed three times with 0.22-μm filtered bidistilled water. The grids were allowed to dry and were visualized in a Philips CM100 transmission electron microscope (accelerating voltage 80 kV).

Results and discussion

Because the monomer misfolding is the well-accepted starting point of the amyloid aggregation process [7,18,32,33], a conformationally homogeneous Aβ42 starting sample is a prerequisite for a reproducible polymerization process. Therefore, on the basis of previous studies [18], the Aβ42 peptide was initially treated with hexafluoroisopropanol (HFIP) to induce a prevalent α-helical structure and the initial conformational homogeneity was evaluated by circular dichroism (CD) spectroscopy. The use of CD was an essential tool to clarify the shift from unordered/α-helix to a β-sheet-rich conformation in amyloid self-assembly. However, to produce morphology-relevant information on high-molecular-weight (HMW) oligomers, the quantitative analysis of monomer disappearance and oligomer formation during the self-assembly process relied on a combination of other more appropriate methods, including MS techniques.

Low-molecular-weight oligomers appear at a very early time of aggregation

HFIP-pretreated Aβ samples, freshly resolubilized in an acetonitrile/alkaline aqueous mixture, were stable and showed a non-amyloidogenic conformation by CD analysis [18], whereas the dilution in phosphate buffer triggered the conformational changes and was taken as $t = 0$ for aggregation studies.

The compliance with the initial Aβ42 monomer status was evaluated and confirmed by MS techniques. The MALDI–TOF mass spectrum of Aβ42 solution at $t = 0$ showed the monomer at 4514 m/z as the most abundant species. More interesting, soon after dilution in phosphate buffer, Aβ monomers tended to associate with short oligomeric species (up to 9 or 10 units) that were detected by MALDI–TOF (Fig. 1). Homogeneously distributed small aggregates with a tendency to form globular and disc-shaped structures were visualized by AFM after deposition on hydrophilic mica surface (Fig. 2, $t = 0$, and Fig. 3A). In less densely populated regions, line analyses were performed and the dimension of these structures was derived (Table 1). A general classification was done by dividing the observed initial oligomeric structures into two classes: (i) a population with an average height of 0.7 ± 0.2 nm ($n = 50$ on three different experiments) and a deconvoluted diameter of 5–10 nm (see Materials and methods) and (ii) a population with a height of 1 to 2 nm and a deconvoluted diameter of 15–25 nm ($n = 75$ on three different experiments). The observed heights of particles, in agreement with previous observations [30,34–37], are relatively constant compared with the apparent diameters. This clearly shows that the lateral dimensions of these particles are not proportional to their heights.

A fast interaction of Aβ42 monomers in an aqueous environment is in agreement with recently published data that propose an initial fast hydrophobic collapse, resulting in the formation of transient spherical oligomers [38]. These oligomeric nuclei were the most abundant species during the very early phase of

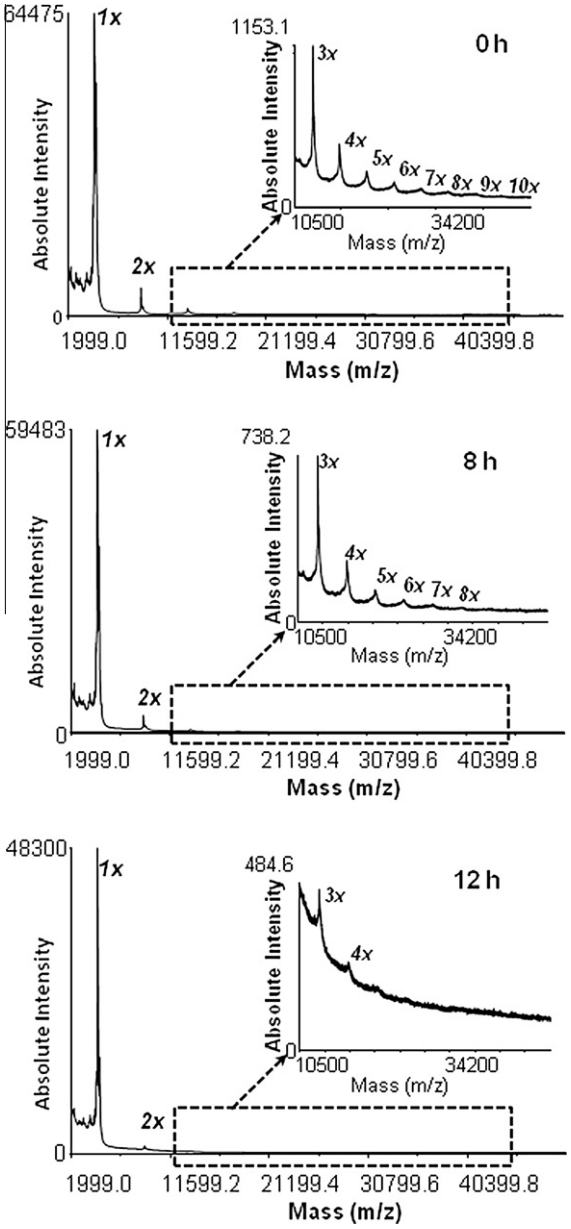

Fig.1. MALDI–TOF analyses of Aβ42. The insets show small oligomer profiles with ⩾3 units at increasing incubation times.

aggregation; they could be reverted to monomers by dilution or transformed into lengthy protofibrils by incubation. Indeed, AFM studies of diluted samples showed a reduction in the relative abundance of short oligomers compared with stable longer intermediates (data not shown). Fluorescence signal in the ThT assay is almost negligible during this initial phase because no ordered oligomeric structures are formed yet. Concerning secondary structure, previous CD studies [18] revealed unordered/α-helix conformation of amyloid sample solution in this early step of the aggregation pathway (Table 1).

The kinetics of oligomerization follows a nucleation-dependent profile

After dilution in phosphate buffer, the Aβ self-assembly process was monitored over time by combining MS techniques (MALDI–TOF, ESI–QTOF, and ESI–IT), microscopy, and a ThT-based fluorescence assay.

ThT dye shows a characteristic red shift in the excitation spectrum and an increase in the quantum yield on binding to fibrillar β-sheet structures [21,39,40]. In agreement with previous studies [18] that revealed a CD shift from unordered/α-helix to a β-sheet-rich conformation, the obtained ThT-based fluorescence experimental values fitted into a Boltzmann sigmoidal equation showing an initial lag phase followed by a steep exponential phase up to a plateau (Fig. 4A); the plateau phase started at 22–24 h, whereas the t_{50} (i.e., time at which the signal is half of the maximum value) occurred at 12.5 h.

Aβ42 aggregation was also monitored by evaluating the monomer decrease by ESI–IT MS flow injection analysis. Quantitation of the Aβ42 monomer was carried out without any previous filtration so as to avoid perturbation of the system. Although small oligomers were already present during the early phases, as determined by MALDI–TOF and AFM studies and as reported elsewhere [41], only the monomeric form was detected under the ESI–MS experimental conditions because it is possible that small oligomers could disaggregate during the flow injection and the ESI. The contribution of dimers and longer oligomers to the ESI–MS analyses was excluded based on the ^{13}C isotope distribution investigated by the ESI–QTOF technique (flow injection [see supplementary material for experimental details]). The QTOF mass spectrum of amyloid samples showed an isotope peak separation for the +4 charge state of precisely 0.25 amu, as expected for a monomer in this multicharged state (i.e., in the case of +8 charged state, dimer would be 0.125 amu). The simultaneous presence of monomer and dimer would have given undistinguished isotopic resolution. Hence, quantitation of the Aβ42 soluble forms was performed by ESI–IT MS on the monomer signals deriving from monomers and likely from the soluble small oligomer disaggregation.

When the profiles obtained in MS studies was compared with those resulting from fluorescence studies, a reversed sigmoidal trend was obtained, showing an initial plateau up to 10 h followed by an exponential decrease until monomer disappearance (Fig. 4B). In accordance with this result, MALDI–TOF studies showed a progressive decrease in the monomer content and the disappearance of short oligomers within 12 h, when only traces of monomer, dimmer, and trimer were found (Fig. 1).

Although the presence of HMW oligomers, protofibrils, and fibrils could not be detected by MALDI–TOF because of their low ionization ability, they were well visualized by microscopy techniques. In particular, at early time, morphology studies on oligomeric and fibrillar structures were mainly carried out by AFM (Fig. 2) because small oligomers were not well resolved by TEM (Fig. 5), likely due to the lower resolution of TEM.

Short oligomers, protofibrils, and some small fibrillar species were simultaneously present during the oligomerization phase, but the prevalence of a species over the others changed over time. It appears, as supported by evidence from the independent methods used here, that a progressive increase in the percentage of organized oligomers and protofibrils occurs over time. Thanks to high resolution of acquired images, AFM analyses allowed the detailed morphological identification of the different aggregated species. Examples of protofibrils [35,37,42–44] formed during the initial phases of aggregation are presented in Fig. 3B. Their heights ranged between 1 and 3 nm, and their widths ranged between 5 and 10 nm (n = 30 on three different experiments [Table 1]), similar to results reported by others [28,45].

On the basis of recently published molecular dynamic simulations [38] and PICUP (photo-induced cross-linking of unmodified proteins) studies [46], Aβ42 has a high propensity to form roundish nuclei that could self-associate into higher order oligomers. In our investigation, these nuclei correspond to the soluble roundish aggregates with molecular weight (MW) up to 45 kDa (MALDI–TOF analyses) whose morphology was well

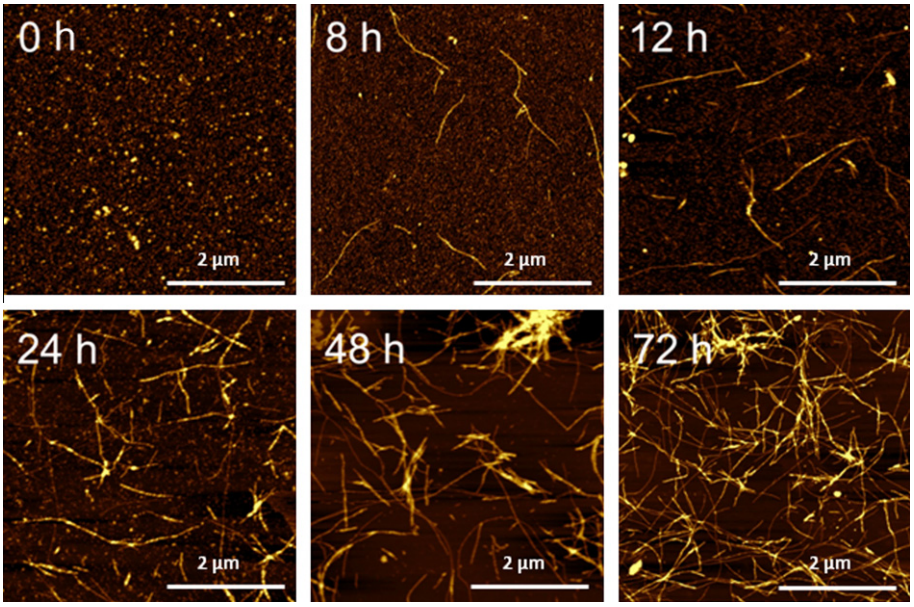

Fig.2. Tapping mode AFM analyses of Aβ42 aggregation kinetics. The images are representative of those in each of at least three independent experiments.

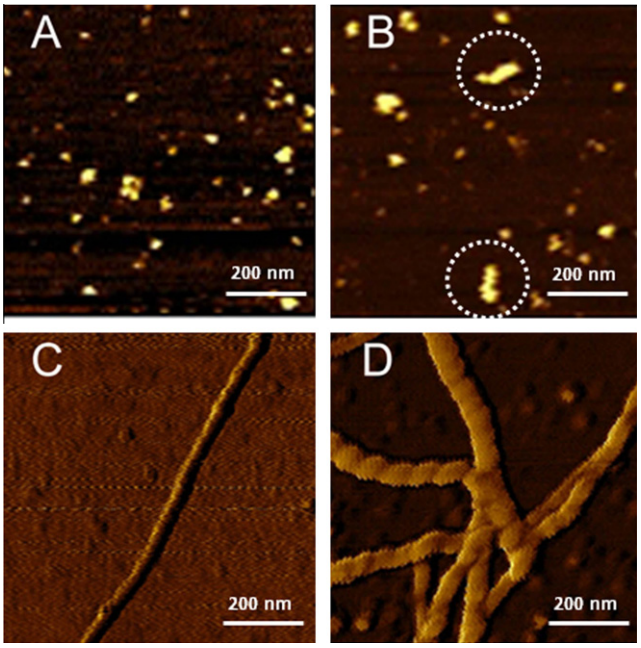

Fig.3. Magnified AFM images showing different morphological species: (A) Aβ42 globular oligomers; (B) protofibrils; (C) smooth fibrils; (D) nodular fibrils.

defined by AFM (Table 1) and that evolve into elongated protofibril structures. MALDI–TOF resulted a suitable and easy-to-handle technique to evaluate formation and disappearance of initial transient species that can hardly be detected by other methodologies. Moreover, different from other approaches, MALDI–TOF does not imply long/complex sample treatment or covalent modification of species in solution as in the PICUP method [47].

HMW oligomer distribution and morphology-related information on soluble amyloid oligomers are complementary to data by CD and ThT fluorescence assay, which is one of the most used methods in similar studies but is limited to only quantitative determination of fibril formation.

To date, very few approaches are available to specifically detect soluble amyloid intermediates (e.g., the immunometric approach, which is based on the recognition of specific conformers or soluble aggregates by tailor-made antibodies) [48–50].

Finally, FLM images obtained after staining with ThT dye were able to highlight only the larger fibrillar structures that appear after 48 h of incubation (see Fig. S1 in supplementary material).

Combined MALDI–TOF and AFM results showed that oligomerization does not proceed through the progressive appearance and disappearance of single species (i.e., monomers → dimers → trimers → ⋯ → decamers → longer oligomers → protofibrils → ⋯); rather, it proceeds through parallel pathways where multiple species coexist. Moreover, the Aβ aggregation appears to proceed exponentially rather than linearly; once the stable oligomers reach a critical size and concentration, a rapid inclusion of residual monomers was observed with a rapid growth of more organized and insoluble structures and fibrils.

At this point, quantitative analyses by ThT-based assay, as well as by ESI–IT and MALDI–TOF (Figs. 1 and 4) and microscopy studies, showed that the amount of monomers and short oligomers was very poor.

Table 1
Dimensional analysis of Aβ42 species detected on mica by AFM (data obtained are the averages of $30 \leqslant n \geqslant 78$ measures), MALDI–TOF analyses, and secondary structure characterization by CD [18].

AFM				MALDI-TOF (MW in kDa)	CD (secondary structure)
Time-course species	Height (nm)	Deconvoluted width (nm)	Length		
LMW oligomers	0.5–0.9	5–10	Globular and disc-shaped	4–56 (1–10 units)	Unordered/α-helix
	1–2	15–25			Unordered/α-helix
Protofibrils	1–3	5–10	>110 nm		β-sheet
Smooth fibrils	0.7–6	8–19	⩽10 μM		
Nodular fibrils	7–12	20–30			

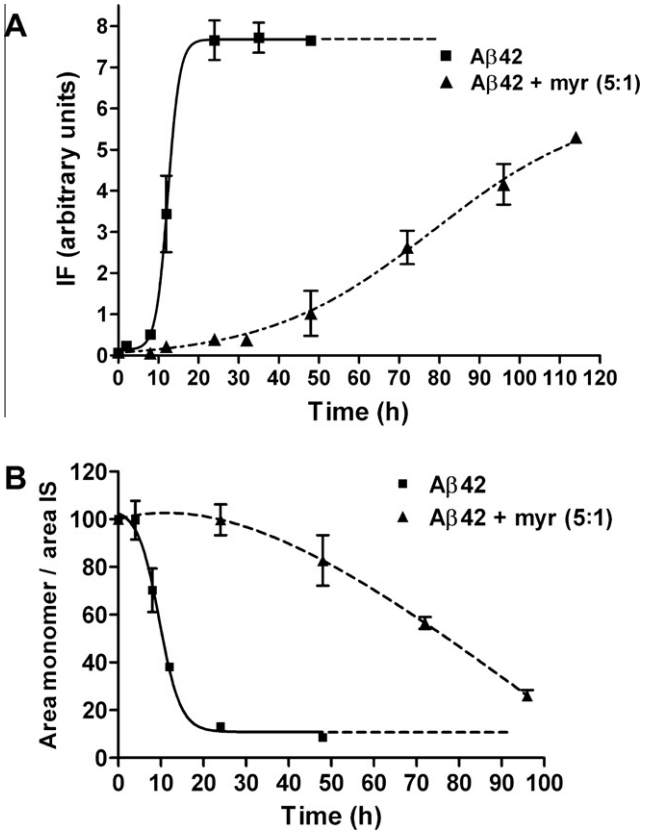

Fig.4. Time course of Aβ42 (50 μM) aggregation in the absence and presence of myricetin (myr, 10 μM) added at $t = 0$. (A) ThT fluorescence profile over time. Samples were incubated at 30 °C and diluted with 1.5 μM ThT before reading; IF = intensity of fluorescence. (B) Monomer time course decrease by ESI–IT. Quantitation was carried out by using reserpine as IS.

Corroborating this evidence, microscopy techniques (Figs. 2 and 5) showed that after 48 h of incubation, Aβ42 samples were almost entirely aggregated into fibrils, whereas the content of monomers, small oligomers, and protofibrils was very low. Because surface coverage was highly reduced, it can be hypothesized that most of them were incorporated into larger fibrils.

The findings described here merge with the previously described three-step sigmoid profile obtained by CD studies [18] that is characterized by a lag phase (prevailing unordered/α-helix conformation), an exponential growth phase (increasing β-sheet secondary structure), and a plateau phase (prevailing β-sheet secondary structure) (Table 1).

Ordered smooth and nodular fibrils form rapidly by inclusion of short oligomers and residual monomers

Chosen experimental conditions led to well morphologically defined fibrils, which can be divided into two main types: smooth (Fig. 3C) and nodular (Fig. 3D), with the latter indicative of high-order supramolecular organization. Smooth fibrils have heights ranging from 0.7 to 6 nm and widths ranging from 8 to 19 nm ($n = 78$ on three independent experiments). Nodular fibrils showed left-handed coiling, with an average height of 9.5 ± 2.5 nm and an average width of 25 ± 5 nm. Both fibril types appeared from the early phase of aggregation (from $t = 4$ h) and were observed to grow in number and length with time, reaching the maximum value (i.e., length of 10 μM) at 24 h.

As a final remark, the general findings obtained with this multimethodological approach are in agreement with the existence of three distinct processes occurring sequentially within the Aβ42 assembly pathway as recently suggested on the basis of computation studies [38]: (i) fast hydrophobic collapse resulting in a population of oligomers that are visualized soon after dilution in buffer as roundish species by AFM and contain up to 10 Aβ42 units (MALDI–TOF), (ii) desolvation enabling charged residues to interact electrostatically and so induce the formation of elongated protofibrils (AFM), and (iii) emergence of parallel in-register intermolecular hydrogen bonding associated with the cross-β structure of the amyloid fibril (TEM, AFM, and FLM).

Microscopy images mirror the distribution of species in the solution

AFM results showed that amyloid species are rapidly trapped on the mica surface. Indeed, increasing the contact time (drying time)

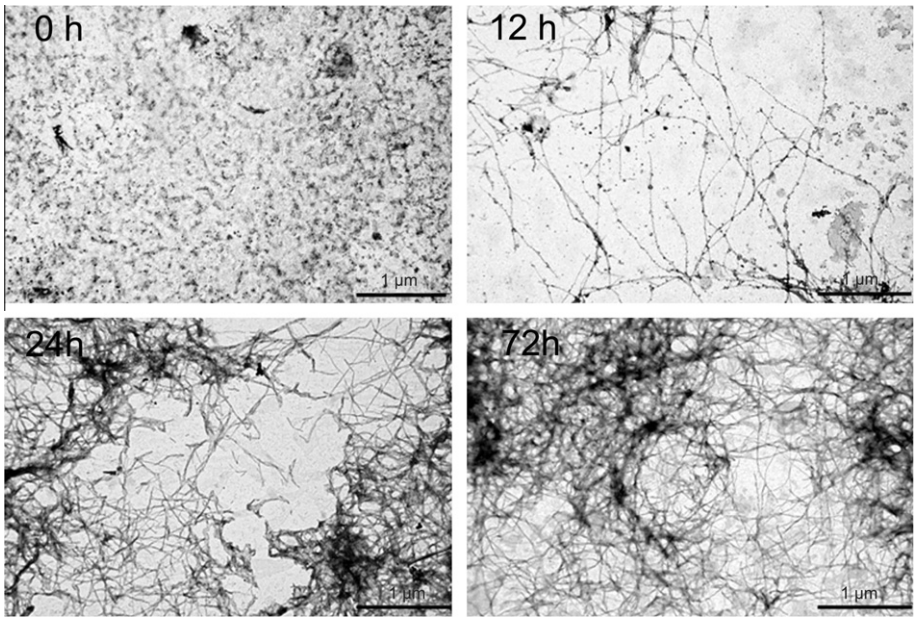

Fig.5. TEM images of Aβ42 aggregation kinetics. Images were acquired after negative staining with 1% aqueous solution of uranyl acetate.

between β-amyloid solution and the mica surface during AFM sample preparation did not produce any change either in the relative abundance of different Aβ species or in their morphology (data not shown). Due to the fast interaction of amyloid with mica surface and the short contact time (1 min) before drying, we hypothesized that the surface-promoting effect encountered in other studies [51] could be excluded. The parallel TEM investigation further corroborated this hypothesis; the TEM images acquired in parallel with AFM confirmed the same degree of polymerization in terms of fibril size and number in the kinetic investigation (e.g., cf. Figs. 2 and 5). These observations allowed us to infer that in our experimental conditions, polymerization occurred in solution without any discernible surface-induced effect.

TEM was also useful for confirming the random orientation of the fibrils observed in AFM images. More interesting, in comparing the overall species profile of negatively stained TEM grids and AFM images, we found a consistency in the morphology and size of the detected species, leading us to the conclusion that AFM images were snapshots of the process in solution.

In Fig. 6, a scheme of the overall Aβ42 aggregation process is displayed together with area of optimal application of the methodologies employed in this study for the integrated characterization of the Aβ42 assembly states.

From the point of view of the information content, the proposed methods can be divided into quantitative (ThT assay, CD, and ESI–MS), semiquantitative (MALDI–TOF), and morphological (AFM, TEM, and FLM) methods. However, as shown in Fig. 6, some reported techniques overlap partially. In particular, among morphological methods, FLM is redundant when TEM and AFM are available. Information recruited by FLM is limited because only large fibrils can be visualized. Furthermore, although TEM and AFM results were equally informative on the protofibril/fibril structure morphology, only AFM offers a suitable image resolution to provide the accurate determination of short oligomers and protofibril shape and dimension. From a quantitative or semiquantitative point of view, and dealing with oligomers, MALDI–TOF can give a valuable characterization of low-molecular-weight (LMW) oligomers and semiquantitative information on the internal ratio of LMW species versus monomer, which is important information in a toxicity study. Monomer quantitative determination by ESI–MS can be well performed with an IT analyzer in SIM mode. In this respect, ESI–QTOF gave a contribution in confirming the monomer multicharged identity, and it was intended as a validating technique for the ESI–IT method. Therefore, each of the two ESI methods can be alternatively used to quantitate monomer content in amyloid samples. Moreover, although MALDI–TOF and ESI–MS analyses are complementary to CD studies because all three methods are focused on monomer characterization, CD is the only technique able to give information on the secondary structure.

Therefore, at the end of these considerations, to properly follow all the stages of amyloid self-assembly, it might be recommended to use (i) a quantitative method such as MS for monomer (ESI–MS) and LMW oligomer characterization and determination (MALDI–TOF is useful for both monomer and LMW oligomers) or ThT for fibril formation, (ii) CD spectroscopy to acquire information on monomers' secondary structure changes, and (iii) a morphological technique (AFM/TEM) to follow small and large species formation and disappearance.

By adding important information on the early phases of the aggregation kinetics from both the quantitative and qualitative points of view, we considered that this approach could be useful in characterizing the mechanism of action of new inhibitors.

Inhibition studies

A reproducible aggregation assay offering a high degree of information is a prerequisite for the reliable characterisation of new inhibitors of the amyloid aggregation process. It must be emphasized that most of published compounds endowed with an antiaggregating action were investigated for their overall effect on the aggregation process rather than for their detailed interaction with specific prefibrillar species [52–54]. In the light of the accepted hypothesis that toxicity is related to specific intermediates [55], the detailed characterization of the mode of action of new inhibitors along all phases of self-assembly is required. Although ThT fluorescence is the most widely used technique for inhibition studies, it must be underlined that a native fluorescence of the inhibitor and/or competition for the same binding site on oligomers/fibrils may provide misleading results if not accounted for properly.

On the basis of these considerations, we applied the described multimethodological approach to characterize the mode of inhibition of myricetin, a well-known natural polyphenol that acts as an inhibitor of Aβ aggregation (see Fig. S2 in supplementary material) [56]. Recent studies on transgenic mice (Tg2576) showed that a prolonged administration of myricetin by mouth increased the levels of soluble Aβ monomers and significantly decreased the amount of fibril deposits [57]. CD spectroscopy confirmed that myricetin was able to prevent structural changes in Aβ42 and to reduce ThT signal after 48 h [58].

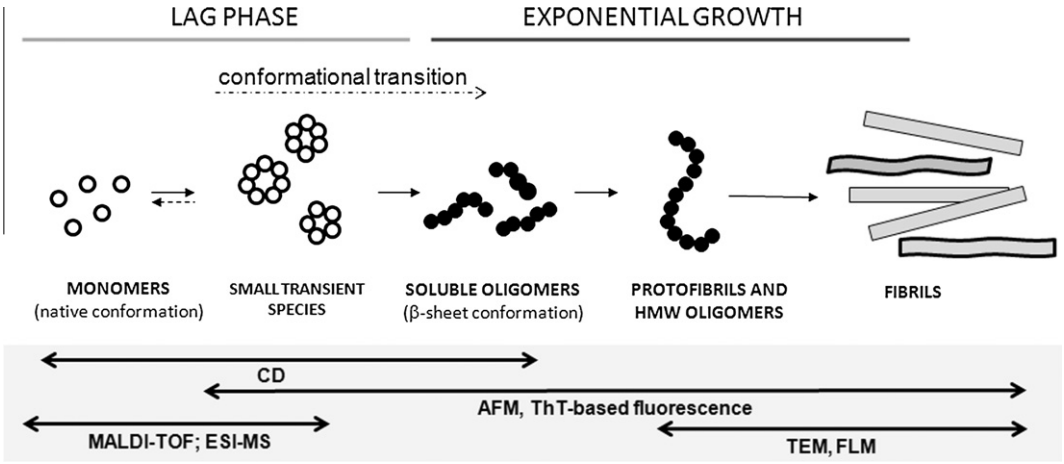

Fig.6. Scheme of the Aβ42 self-assembly process. Suitable techniques for morphological and/or quantitative evaluation of prevailing species at different phases of the aggregation process are shown.

As a starting point, the inhibitory potency of myricetin in our experimental conditions was initially determined by ThT-based assay. The resulting IC_{50} value was 2.60 ± 0.33 μM (see supplementary material for details), whereas at 10 μM myricetin was able to inhibit almost completely (94.1 ± 0.5%) the increase of the fluorescence signal at 490 nm related to Aβ42 aggregation after 24 h of incubation. A 10-μM concentration was used for further experiments with the multimethodological approach to maximize differences between the inhibitor-free samples and samples treated with inhibitor.

In agreement with a stabilizing action on Aβ monomers [58], the results reported here showed that, in the presence of myricetin, the overall assembly process was greatly retarded and fibril formation was strongly delayed. Myricetin decreased the ThT fluorescence associated with Aβ fibrils, resulting in a shift of the t_{50} from 12.5 to 78.5 h (Fig. 4A). In agreement with this result, monomer quantitation by ESI–IT MS showed a similar t_{50} shift from 9.6 to 73.8 h (Fig. 4B). At 24 h, residual monomer content was 13.8% and 94.7% in the absence and presence of myricetin, respectively. In agreement with the above data, the MALDI–TOF profile at 24 h in the presence of myricetin still shows a high content of LMW oligomers, confirming that the amyloid aggregation is still in its very early phase (data not shown). Quantitative analyses of LMW oligomer/monomer content over time (Fig. 7A) show that

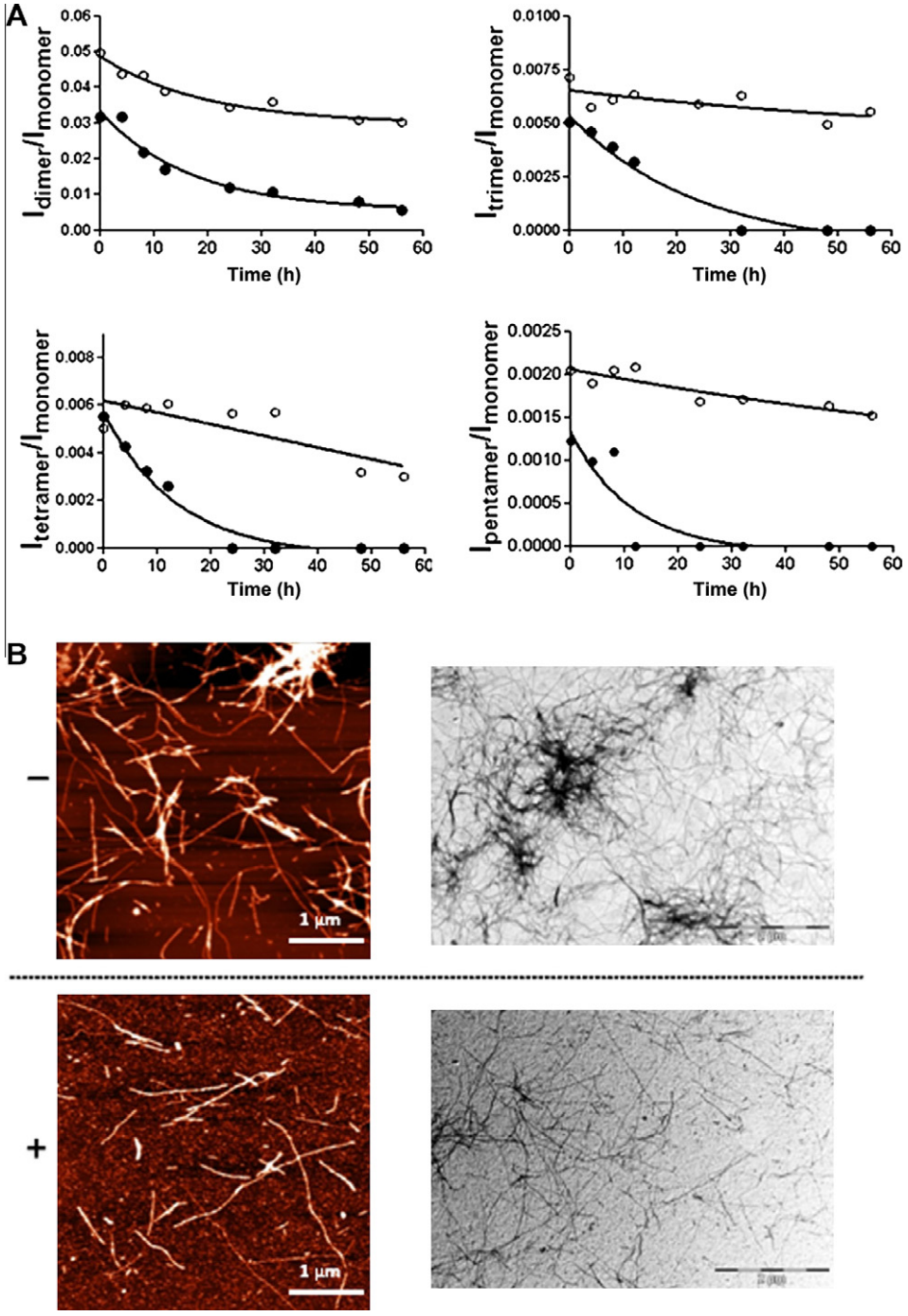

Fig.7. (A) Time course trend of Aβ42 dimer, trimer, tetramer, and pentamer/monomer absolute intensity with (○) and without (●) myricetin by MALDI–TOF. (B) AFM and TEM images at 48 h of Aβ42 with (+) and without (–) myricetin.

myricetin strongly delays the transition from short oligomers to more organized soluble intermediates. Moreover, in inspecting AFM and TEM images acquired at 48 h of incubation, small oligomers were still well detectable in samples containing myricetin, whereas only highly ordered structures were present in samples with Aβ42 alone (Fig. 7B). Thus, the morphological and quantitative data by multiple techniques univocally confirmed that myricetin disrupts folding and avoids the deposition of ordered structures with changes in the morphology of the various species. As a further conclusion, data obtained with MS and microscopy techniques fully confirmed results from the ThT-based assay and allowed excluding false positives and false negatives.

Furthermore, the high reproducibility of the aggregation process and the possibility of monitoring the appearance and disappearance of the intermediate species during amyloid aggregation allow further investigation on the specific targeted monomeric/oligomeric form by adding the inhibitor at different times during the aggregation process.

Specifically, other than at $t = 0$, myricetin was also added at t_{50} (half-time course in ThT assay, corresponding to growing oligomers) and t_{90} (time corresponding to 90% of the exponential increase of the fluorescence signal in the ThT assay), and the effects on the progression of Aβ aggregation were evaluated. The results presented showed that myricetin interfered with the formation of protofibrils and the subsequent progression to fibrils even if added when the transition toward stable longer oligomeric species has started (see Fig. S4 in supplementary material). In this case, the observed retarding effect is higher when addition is carried out at an early time. When added at t_{90} (higher content of fibrils), myricetin was not able to reverse the aggregation process or disaggregate the already formed HMW species and fibrils. Instead, it was able to strongly slow down further elongation.

To sum up, the results strongly indicate that the species targeted by myricetin is the Aβ monomer in the non-aggregation-prone conformation (low level of β-sheet content) and short transient oligomers, which are predominant during the first hours of the self-assembly process and slowly disappear when Aβ fibrils become prevalent.

Finally, to further validate this multimethodological approach, tacrine (see Fig. S2), an anticholinesterase drug used in the past for AD treatment was selected as a negative control because it was previously demonstrated that tacrine is not effective in perturbing spontaneous amyloid assembly [18]. Analyses were performed using the same experimental conditions. Neither changes of the Aβ sigmoid trend nor any variation of relative self-assembly states was observed in the presence of this compound. As further evidence, a significant decrease in ThT fluorescence did not occur in the presence of tacrine after 24 h, and MALDI–TOF profiles did not differ from those obtained with the tacrine-free Aβ42 sample (data not shown).

Conclusions

The limited access to characterization of the earliest events of Aβ42 aggregation suggests the need for a deeper multitechnique study to bridge the experimental gap between the monomer and fibril endpoints. Results obtained in this work translate into the development of a reproducible Aβ42 aggregation protocol that would allow the characterization of the different assembly species and the definition of their morphology, MW, and relative abundance. This information is crucial to avoid confusing outcomes from both aggregation studies and screening of inhibitors.

The multimethodological approach presented here provides a clearer and more consistent picture of the in vitro Aβ42 aggregation process by detailing the diverse assembly species, which are formed from the early stages to fibrilization. A striking result is the characterization of the morphology and MW of the nucleant species by AFM and MALDI–TOF. Of particular note is the quantitative applicative aspect of the proposed methodologies that confers a suitable reliability for the definition of the potency and mode of action of newly identified inhibitors.

Concerning the use of a multimethodological approach for screening new antiaggregating agents, some considerations are worth doing. Because the full characterization of a new compound is costly and time-consuming, a step-by-step process, in which a number of new potential inhibitors are first screened and only the most promising ones are further characterized, is usually pursued. In the light of this general modus operandi, a similar sequential approach can be suggested when antiaggregating agents are studied.

For an initial high-throughput screening (HTS) approach, the ThT-based assay is a well-suited quantitative technique because it affords the screening of a high number of new molecular entities and the selection of active compounds. On the other hand, the ThT approach cannot be applied when dealing with compounds showing absorption or quenching phenomena at the selected assay wavelength, thereby generating false positive and false negative results, respectively. Analyses by an independent technique at a fixed time of incubation may be useful to confirm the inhibitory properties before further investigation. Then, once the most active hits are selected, a deeper investigation can provide information on the mechanism of action. Quantitative kinetic information on the conformational changes over oligomerization and aggregation can be obtained by CD analysis. The selectivity of ThT binding for fibrils suggests that active compounds resulting in this assay interfere with fibril formation without any information on the amyloid species targeted by the inhibitor. On the other hand, compounds able to alter the conformational shift amyloid peptides (CD studies) might block or slow the early phases of Aβ oligomerization. The same quantitative information on monomer content can be given by ESI–MS. Therefore, a combination of ThT assay and ESI analysis or CD studies may give reliable information on the inhibitor concentration needed to stop the overall fibrilization process (ThT) and weather the inhibitor is able to freeze the monomeric form of Aβ (CD or ESI–IT). Then MALDI–TOF MS can be used to confirm that the increase in monomers decreases the formation of short oligomers at specific time intervals in view of an inhibitor effect on toxicity due to oligomers.

To sum up, a schematic procedure for inhibitor evaluation could be as follows: (i) fast screen new compounds by a ThT assay and select the ones that show IC_{50} values in the low micromolar range, (ii) validate the ThT data with an independent technique at a fixed time of incubation (morphological as AFM or TEM or quantitative) to avoid misleading data, and (iii) investigate in detail the mechanism of action by monitoring the effect of the inhibitor on the formation of the different oligomeric species over time. CD, MALDI–TOF MS or ESI–MS, and microscopy methods can be selected and combined depending on instrument availability.

Concerning the inhibitor selected in this study, results strongly indicate that the species preferentially targeted by myricetin are the Aβ monomers and short transient oligomers. Myricetin was able to interfere with the progression of the Aβ42 aggregation process even if added when the conformational transition and monomer oligomerization had started. Therefore, it is conceivable that myricetin would be more efficient as early therapy instead of as reversing an already started aggregation cascade.

Finally, the same approach can be extended to the aggregation of many other aggregation-prone peptides because most peptides involved in human aggregation diseases display similar aggregation features and intermediates [59].

Acknowledgments

This work was supported by a European funded FP7 grant (Bio-Inspired Self-Assembled Nano-Enabled Surfaces [BISNES]). The University of Bologna (RFO) is also gratefully acknowledged for its financial support. Finally, the authors kindly acknowledge Maria Roberta Randi and Davide Cavalletti for their technical assistance in electron microscopy and fluorescence microscopy, respectively.

Appendix A. Supplementary data

Supplementary data associated with this article can be found, in the online version, at doi:10.1016/j.ab.2011.03.020.

References

[1] J. Naslund, V. Haroutunian, R. Mohs, K.L. Davis, P. Davies, P. Greengard, J.D. Buxbaum, Correlation between elevated levels of amyloid β-peptide in the brain and cognitive decline, JAMA 283 (2000) 1571–1577.
[2] D.J. Selkoe, Alzheimer's disease results from the cerebral accumulation and cytotoxicity of amyloid β-protein, J. Alzheimer's Dis. 3 (2001) 75–80.
[3] D.J. Selkoe, Translating cell biology into therapeutic advances in Alzheimer's disease, Nature 399 (1999) A23–A31.
[4] M.A. Findeis, The role of amyloid beta peptide 42 in Alzheimer's disease, Pharmacol. Ther. 116 (2007) 266–286.
[5] D. Scheuner, C. Eckman, M. Jensen, X. Song, M. Citron, N. Suzuki, T.D. Bird, J. Hardy, M. Hutton, W. Kukull, E. Larson, E. Levy-Lahad, M. Viitanen, E. Peskind, P. Poorkaj, G. Schellenberg, R. Tanzi, W. Wasco, L. Lannfelt, D. Selkoe, S. Younkin, Secreted amyloid β-protein similar to that in the senile plaques of Alzheimer's disease is increased in vivo by the presenilin 1 and 2 and APP mutations linked to familial Alzheimer's disease, Nat. Med. 2 (1996) 864–870.
[6] T. Luhrs, C. Ritter, M. Adrian, D. Riek-Loher, B. Bohrmann, H. Dobeli, D. Schubert, R. Riek, 3D structure of Alzheimer's amyloid-β (1-42) fibrils, Proc. Natl. Acad. Sci. USA 102 (2005) 17342–17347.
[7] D.M. Walsh, D.J. Selkoe, Oligomers on the bra, in: The emerging role of soluble protein aggregates in neurodegeneration, Protein Pept. Lett. 11 (2004) 213–228.
[8] C.G. Glabe, R. Kayed, Common structure and toxic function of amyloid oligomers implies a common mechanism of pathogenesis, Neurology 66 (2006) S74–S78.
[9] M.P. Lambert, A.K. Barlow, B.A. Chromy, C. Edwards, R. Freed, M. Liosatos, T.E. Morgan, I. Rozovsky, B. Trommer, K.L. Viola, P. Wals, C. Zhang, C.E. Finch, G.A. Krafft, W.L. Klein, Diffusible nonfibrillar ligands derived from Aβ1-42 are potent central nervous system neurotoxins, Proc. Natl. Acad. Sci. USA 95 (1998) 6448–6453.
[10] D.M. Walsh, I. Klyubin, J.V. Fadeeva, W.K. Cullen, R. Anwyl, M.S. Wolfe, M.J. Rowan, D.J. Selkoe, Naturally secreted oligomers of amyloid beta protein potently inhibit hippocampal long-term potentiation in vivo, Nature 416 (2002) 535–539.
[11] S. Varadarajan, S. Yatin, M. Aksenova, D.A. Butterfield, Alzheimer's amyloid β-peptide-associated free radical oxidative stress and neurotoxicity [review], J. Struct. Biol. 130 (2000) 184–208.
[12] M. Sandal, F. Valle, I. Tessari, S. Mammi, E. Bergantino, F. Musiani, M. Brucale, L. Bubacco, B. Samori, Conformational equilibria in monomeric ββ-synuclein at the single-molecule level, PLoS Biol. 6 (2008) e6.
[13] P. Hortschansky, V. Schroeckh, T. Christopeit, G. Zandomeneghi, M. Fandrich, The aggregation kinetics of Alzheimer's β-amyloid peptide is controlled by stochastic nucleation, Protein Sci. 14 (2005) 1753–1759.
[14] M. Necula, R. Kayed, S. Milton, C.G. Glabe, Small molecule inhibitors of aggregation indicate that amyloid beta oligomerization and fibrillization pathways are independent and distinct, J. Biol. Chem. 282 (2007) 10311–10324.
[15] M. Zhu, S. Han, F. Zhou, S.A. Carter, A.L. Fink, Annular oligomeric amyloid intermediates observed by in situ atomic force microscopy, J. Biol. Chem. 279 (2004) 24452–24459.
[16] S.A. Moore, T.N. Huckerby, G.L. Gibson, N.J. Fullwood, S. Turnbull, B.J. Tabner, O.M. El-Agnaf, D. Allsop, Both the D-(+) and L-(−) enantiomers of nicotine inhibit Aβ aggregation and cytotoxicity, Biochemistry 43 (2004) 819–826.
[17] T. Kihara, S. Shimohama, A. Akaike, Effects of nicotinic receptor agonists on β-amyloid β-sheet formation, Jpn. J. Pharmacol. 79 (1999) 393–396.
[18] M. Bartolini, C. Bertucci, M.L. Bolognesi, A. Cavalli, C. Melchiorre, V. Andrisano, Insight into the kinetic of amyloid beta (1-42) peptide self-aggregation: Elucidation of inhibitors' mechanism of action, Chem. Bio. Chem. 8 (2007) 2152–2161.
[19] D.A. Middleton, Solid-state NMR spectroscopy as a tool for drug design: From membrane-embedded targets to amyloid fibrils, Biochem. Soc. Trans. 35 (2007) 985–990.
[20] H. Inouye, D.A. Kirschner, Alzheimer's β-amyloid: Insights into fibril formation and structure from Congo red binding, Subcell. Biochem. 38 (2005) 203–224.
[21] H. Naiki, F. Gejyo, Kinetic analysis of amyloid fibril formation, Methods Enzymol. 309 (1999) 305–318.
[22] D.H. Anderson, K.C. Talaga, A.J. Rivest, E. Barron, G.S. Hageman, L.V. Johnson, Characterization of beta amyloid assemblies in drusen: The deposits associated with aging and age-related macular degeneration, Exp. Eye Res. 78 (2004) 243–256.
[23] G. Bitan, E.A. Fradinger, S.M. Spring, D.B. Teplow, Neurotoxic protein oligomers: What you see is not always what you get, Amyloid 12 (2005) 88–95.
[24] X.P. Wang, J.H. Zhang, Y.J. Wang, Y. Feng, X. Zhang, X.X. Sun, J.L. Li, X.T. Du, M.P. Lambert, S.G. Yang, M. Zhao, W.L. Klein, R.T. Liu, Conformation-dependent single-chain variable fragment antibodies specifically recognize β-amyloid oligomers, FEBS Lett. 583 (2009) 579–584.
[25] C. Goldsbury, P. Frey, V. Olivieri, U. Aebi, S.A. Muller, Multiple assembly pathways underlie amyloid-β fibril polymorphisms, J. Mol. Biol. 352 (2005) 282–298.
[26] N. Benseny-Cases, M. Cocera, J. Cladera, Conversion of non-fibrillar β-sheet oligomers into amyloid fibrils in Alzheimer's disease amyloid peptide aggregation, Biochem. Biophys. Res. Commun. 361 (2007) 916–921.
[27] I. Tessari, M. Bisaglia, F. Valle, B. Samori, E. Bergantino, S. Mammi, L. Bubacco, The reaction of ββ-synuclein with tyrosinase: Possible implications for Parkinson disease, J. Biol. Chem. 283 (2008) 16808–16817.
[28] M. Arimon, I. Diez-Perez, M.J. Kogan, N. Durany, E. Giralt, F. Sanz, X. Fernandez-Busquets, Fine structure study of Aβ1-42 fibrillogenesis with atomic force microscopy, FASEB J. 19 (2005) 1344–1346.
[29] G. Drochioiu, M. Manea, M. Dragusanu, M. Murariu, E.S. Dragan, B.A. Petre, G. Mezo, M. Przybylski, Interaction of β-amyloid(1-40) peptide with pairs of metal ions: An electrospray ion trap mass spectrometric model study, Biophys. Chem. 144 (2009) 9–20.
[30] W.B. Stine Jr., S.W. Snyder, U.S. Ladror, W.S. Wade, M.F. Miller, T.J. Perun, T.F. Holzman, G.A. Krafft, The nanometer-scale structure of amyloid-β visualized by atomic force microscopy, J. Protein Chem. 15 (1996) 193–203.
[31] J. Vesenka, M. Guthold, C.L. Tang, D. Keller, E. Delaine, C. Bustamante, Substrate preparation for reliable imaging of DNA molecules with the scanning force microscope, Ultramicroscopy 42-44 (1992) 1243–1249.
[32] M. Yang, D.B. Teplow, Amyloid β-protein monomer folding: Free-energy surfaces reveal alloform-specific differences, J. Mol. Biol. 384 (2008) 450–464.
[33] R. Roychaudhuri, M. Yang, M.M. Hoshi, D.B. Teplow, Amyloid β-protein assembly and Alzheimer disease, J. Biol. Chem. 284 (2009) 4749–4753.
[34] A. Parbhu, H. Lin, J. Thimm, R. Lal, Imaging real-time aggregation of amyloid beta protein (1-42) by atomic force microscopy, Peptides 23 (2002) 1265–1270.
[35] J.D. Harper, S.S. Wong, C.M. Lieber, P.T. Lansbury Jr., Assembly of Aβ amyloid protofibrils: An in vitro model for a possible early event in Alzheimer's disease, Biochemistry 38 (1999) 8972–8980.
[36] M.P. Lambert, K.L. Viola, B.A. Chromy, L. Chang, T.E. Morgan, J. Yu, D.L. Venton, G.A. Krafft, C.E. Finch, W.L. Klein, Vaccination with soluble Aβ oligomers generates toxicity-neutralizing antibodies, J. Neurochem. 79 (2001) 595–605.
[37] J.D. Harper, S.S. Wong, C.M. Lieber, P.T. Lansbury, Observation of metastable Aβ amyloid protofibrils by atomic force microscopy, Chem. Biol. 4 (1997) 119–125.
[38] B. Urbanc, M. Betnel, L. Cruz, G. Bitan, D.B. Teplow, Elucidation of amyloid β-protein oligomerization mechanisms: Discrete molecular dynamics study, J. Am. Chem. Soc. 132 (2010) 4266–4280.
[39] M. Groenning, L. Olsen, M. van de Weert, J.M. Flink, S. Frokjaer, F.S. Jorgensen, Study on the binding of thioflavin T to β-sheet-rich and non-β-sheet cavities, J. Struct. Biol. 158 (2007) 358–369.
[40] H. Naiki, K. Higuchi, M. Hosokawa, T. Takeda, Fluorometric determination of amyloid fibrils in vitro using the fluorescent dye, thioflavin T1, Anal. Biochem. 177 (1989) 244–249.
[41] S.L. Bernstein, T. Wyttenbach, A. Baumketner, J.E. Shea, G. Bitan, D.B. Teplow, M.T. Bowers, Amyloid β-prote, in: Monomer structure and early aggregation states of Aβ42 and its Pro19 alloform, J. Am. Chem. Soc. 127 (2005) 2075–2084.
[42] D.M. Walsh, D.M. Hartley, Y. Kusumoto, Y. Fezoui, M.M. Condron, A. Lomakin, G.B. Benedek, D.J. Selkoe, D.B. Teplow, Amyloid β-protein fibrillogenesis: Structure and biological activity of protofibrillar intermediates, J. Biol. Chem. 274 (1999) 25945–25952.
[43] J.D. Harper, C.M. Lieber, P.T. Lansbury Jr., Atomic force microscopic imaging of seeded fibril formation and fibril branching by the Alzheimer's disease amyloid-β protein, Chem. Biol. 4 (1997) 951–959.
[44] D.M. Walsh, A. Lomakin, G.B. Benedek, M.M. Condron, D.B. Teplow, Amyloid β-protein fibrillogenesis: Detection of a protofibrillar intermediate, J. Biol. Chem. 272 (1997) 22364–22372.
[45] I.A. Mastrangelo, M. Ahmed, T. Sato, W. Liu, C. Wang, P. Hough, S.O. Smith, High-resolution atomic force microscopy of soluble A842 oligomers, J. Mol. Biol. 358 (2006) 106–119.
[46] G. Bitan, M.D. Kirkitadze, A. Lomakin, S.S. Vollers, G.B. Benedek, D.B. Teplow, Amyloid β-protein (Aβ) assembly: Aβ 40 and Aβ 42 oligomerize through distinct pathways, Proc. Natl. Acad. Sci. USA 100 (2003) 330–335.
[47] G. Bitan, Structural study of metastable amyloidogenic protein oligomers by photo-induced cross-linking of unmodified proteins, Methods Enzymol. 413 (2006) 217–236.
[48] R. Kayed, E. Head, J.L. Thompson, T.M. McIntire, S.C. Milton, C.W. Cotman, C.G. Glabe, Common structure of soluble amyloid oligomers implies common mechanism of pathogenesis, Science 300 (2003) 486–489.
[49] M. Masuda, N. Suzuki, S. Taniguchi, T. Oikawa, T. Nonaka, T. Iwatsubo, S. Hisanaga, M. Goedert, M. Hasegawa, Small molecule inhibitors of ββ-synuclein filament assembly, Biochemistry 45 (2006) 6085–6094.

[50] J.P. Cleary, D.M. Walsh, J.J. Hofmeister, G.M. Shankar, M.A. Kuskowski, D.J. Selkoe, K.H. Ashe, Natural oligomers of the amyloid-β protein specifically disrupt cognitive function, Nat. Neurosci. 8 (2005) 79–84.
[51] L. Hamon, D. Panda, P. Savarin, V. Joshi, J. Bernhard, E. Mucher, A. Mechulam, P.A. Curmi, D. Pastre, Mica surface promotes the assembly of cytoskeletal proteins, Langmuir 25 (2009) 3331–3335.
[52] S.S. Durairajan, Q. Yuan, L. Xie, W.S. Chan, W.F. Kum, I. Koo, C. Liu, Y. Song, J.D. Huang, W.L. Klein, M. Li, Salvianolic acid B inhibits Aβ fibril formation and disaggregates preformed fibrils and protects against Aβ-induced cytotoxicty, Neurochem. Intl. 52 (2008) 741–750.
[53] J.H. Byun, H. Kim, Y. Kim, I. Mook-Jung, D.J. Kim, W.K. Lee, K.H. Yoo, Aminostyrylbenzofuran derivatives as potent inhibitors for Aβ fibril formation, Bioorg. Med. Chem. Lett. 18 (2008) 5591–5593.
[54] S.R. Byeon, J.H. Lee, J.H. Sohn, D.C. Kim, K.J. Shin, K.H. Yoo, I. Mook-Jung, W.K. Lee, D.J. Kim, Bis-styrylpyridine and bis-styrylbenzene derivatives as inhibitors for Aβ fibril formation, Bioorg. Med. Chem. Lett. 17 (2007) 1466–1470.
[55] M. Sakono, T. Zako, Amyloid oligomers: Formation and toxicity of Aβ oligomers, FEBS J. 277 (2010) 1348–1358.
[56] K. Ono, Y. Yoshiike, A. Takashima, K. Hasegawa, H. Naiki, M. Yamada, Potent anti-amyloidogenic and fibril-destabilizing effects of polyphenols in vitro: Implications for the prevention and therapeutics of Alzheimer's disease, J. Neurochem. 87 (2003) 172–181.
[57] T. Hamaguchi, K. Ono, A. Murase, M. Yamada, Phenolic compounds prevent Alzheimer's pathology through different effects on the amyloid-β aggregation pathway, Am. J. Pathol. 175 (2009) 2557–2565.
[58] Y. Shimmyo, T. Kihara, A. Akaike, T. Niidome, H. Sugimoto, Multifunction of myricetin on Aβ: Neuroprotection via a conformational change of Aβ and reduction of Aβ via the interference of secretases, J. Neurosci. Res. 86 (2008) 368–377.
[59] M. Bartolini, V. Andrisano, Strategies for the inhibition of protein aggregation in human diseases, ChemBioChem. 11 (2010) 1018–1035.